

Superexponential Interactions and the Dynamical Unfolding of Confined Degrees of Freedom

Peter Schmelcher^{1, 2, *}

¹*Zentrum für Optische Quantentechnologien, Universität Hamburg,
Luruper Chaussee 149, 22761 Hamburg, Germany*

²*The Hamburg Centre for Ultrafast Imaging, Universität Hamburg,
Luruper Chaussee 149, 22761 Hamburg, Germany*

(Dated: December 2, 2021)

Abstract

We explore a two-body system with superexponential interactions that serves as a fundamental building block for a route to complexity. While being of striking simplicity this highly nonlinear interaction yields a plethora of intriguing properties and a rich dynamics. It exhibits a spatial region where the dynamics occurs in a channel characterised by a transversally confined and longitudinally unbounded motion and additionally two distinct regions where the dynamics is asymptotically free. A deconfinement transition via two saddle points connects the dynamics in the channel with the asymptotically free motion. The scattering functions show plateau and peak structures that can be interpreted in terms of corresponding correlation diagrams. These are intimately related to the varying anharmonicity of the transverse motion while moving along the longitudinal dimension of the channel. We perform a comprehensive analysis of the scattering transition for energies below and above the saddle points. Possible variants and extensions of the superexponential interaction to many-body system are briefly discussed.

* Peter.Schmelcher@physnet.uni-hamburg.de

I. MOTIVATION AND INTRODUCTION

The route of describing nature by a bottom-up approach has been overwhelmingly successful in physics. Elementary constituents and building blocks of matter and their interactions are identified and used to explore the structure and dynamics of composite and more complex systems. This holds for electrons and nuclei forming atoms [1], atoms binding together and forming molecules [2], larger clusters [3] or even nanostructures [4] and crystals [5]. As a matter of fact, the fundamental forces between such elementary constituents are typically of the appearance of an inverse power law such as $\frac{1}{r^2}$ for Coulomb forces among charges and $\frac{1}{r^4}$ for dipolar forces among permanent dipoles. An amazing and seemingly endless complexity of structures and properties emerges from the interaction of many particles via these forces which is responsible for the variety and diversity of phenomena which we observe in nature.

A second well-known bottom-up route to complexity is the coupling of (non-)linear oscillators which describe a plethora of phenomena. For coupled linear oscillators the dynamics is still integrable and describes e.g. the multi-mode small amplitude vibrational dynamics of molecules [6] or phonons in a bulk [5]. Coupled nonlinear and driven oscillators readily lead to a transition from regularity to chaos characterized by a so-called mixed phase space with regular islands, chaotic seas and fractal structures leading to stickiness and Levy flights [7–9]. This extends in (discrete) nonlinear models to localized excitations such as breathers [10] and even phononic frequency combs due to nonlinear resonances [11].

In view of the successful bottom up approach and encouraged by the corresponding emerging complexity, one might ask the following question. Is there other interactions among corresponding fundamental building blocks which would lead us via a different route to a different complex behaviour. Here both the notion of fundamental building blocks and of their interactions is not (necessarily) meant to be of microscopic origin, as it is the case for atoms and their compounds describe above. They could be e.g. the result of an effective theory which incorporates a hierarchy of degrees of freedom describing a highly nonlinear system.

In the above spirit, some preliminary steps have been taken very recently [12, 13]. Firstly a driven power law oscillator [12] has been explored where the exponent of the oscillator

potential is harmonically oscillating in time according to $V(q) \propto |q|^{\beta(t)}$ with $\beta(t) \propto \sin \omega t$ thereby covering a broad spectrum of anharmonicities during the cyclic evolution. This oscillator leads to a two-component phase space. Bounded motion occurs with an underlying mixed regular chaotic phase space and its characteristic dynamical consequences. The second component in phase space corresponds to an unbounded motion which exhibits an exponential net growth of the corresponding energies leading to a tunable exponential acceleration. In a second step the superexponential self-interacting (SSO) oscillator [13] has been introduced and analyzed. For this oscillator both the base and the exponent depend on the dynamical variable (coordinate) of the oscillator leading to the potential $V(q) \propto |q|^q$. In this case it is left to the intrinsic time-evolution of the dynamical oscillator which instantaneous potential it 'feels'. Opposite to standard oscillators such as the (an-)harmonic confining oscillator with $V(q) \propto q^{2n}$ with $n \in \mathbb{N}$ the SSO combines both scattering and confined periodic motion with an exponentially varying nonlinearity. Specifically the SSO potential exhibits a transition point with a hierarchy of singularities of logarithmic and power law character leaving their fingerprints in the agglomeration of its phase space curves. The period of the SSO consequently undergoes a crossover from decreasing linear to a nonlinearly increasing behaviour when passing the transition energy.

In the present work we perform a significant step forward in the above discussed route to complexity. As a key ingredient and building block we introduce a superexponential interaction potential (SEP) $\mathcal{V}(q_i, q_j) = |q_i|^{q_j}$ for the degrees of freedom q_i and q_j . Obviously such an interaction does not respect common symmetries for the fundamental forces in nature such as the translational or permutational invariance. Therefore the degrees of freedom q_i would typically belong to a more complex subunit which we still call in the following (effective) particles. We explore and analyze the two-body problem as a key ingredient for all further investigations on larger systems. The extreme spatially varying nonlinearity of the SEP which is experienced by the particles via their intrinsic dynamics leads to a very rich and uncommon behaviour. The SEP possesses a channel of hybrid confined and unbounded motion with spatially varying anharmonicities which is separated via two saddle points from two regions of unbounded free motion which are separated by a repulsive barrier. We explore the dynamics on the level of single trajectories and ensemble properties below and above

the saddle point energies thereby developing a detailed understanding of the deconfinement transition from confined channel dynamics to the asymptotically free motion. This opens up the perspective of considering the SEP and the many possible modifications of it as a fundamental building block of a dynamical complex network.

In detail we proceed as follows. In section II we describe our setup and analyze the properties of the superexponential two-body potential. This section is central to understand the major differences of the SEP as compared to many standard two-body potentials. Section III contains an elaborate discussion of the dynamics taking place in the SEP. Subsection III A is dedicated to a trajectory-based scattering analysis in the hybrid confining channel below the energy of the saddle points. Subsection III B analyzes the ensemble behaviour in this channel and the most striking properties due to the spatially and dynamically varying anharmonicities. The scattering dynamics for energies above the saddle points leading to a deconfinement transition is investigated in subsection III C. Finally, section IV contains our conclusions and outlook briefly addressing the many perspectives which open up on basis of our two-body investigation. This includes not only the extension to the many-body problem but also the rich possible variations of its two-body ingredient based on the SEP touching upon higher dimensions, varying exponents and geometries.

II. THE SUPEREXPONENTIAL TWO-BODY POTENTIAL

In this section we introduce the Hamiltonian of our two-body problem with superexponential interactions and discuss its major properties. This will serve as a basis for the forthcoming investigations on the dynamics in section III. The Hamiltonian of our two-body problem reads as follows

$$\mathcal{H} = \frac{p_1^2}{2} + \frac{p_2^2}{2} + |q_1|^{q_2} \quad (1)$$

the coordinates q_1, q_2 and their kinetic momenta p_1, p_2 should be considered as belonging to two effective particles or, in general, effective degrees of freedom describing the motion of the fundamental building blocks of our two-body system. The last term of the above Hamiltonian (1) constitutes the superexponential potential $\mathcal{V} = |q_1|^{q_2}$ whose properties are

of central importance to all what follows. In contrast to many well-established fundamental interaction potentials, such as the power law potentials $\propto q^n$ with $n \in \mathbb{Z}$, the SEP possesses a peculiar shape in the sense that both the base and the exponent of it depend on two different dynamical degrees of freedom q_1 and q_2 respectively. This automatically implies that any dynamics taking place in the coordinate q_2 leads to a different potential instantaneously experienced by the degree of freedom q_1 and vice versa. As a result of this superexponential coupling the instantaneous exponent can vary from extremely confining ($q_2 \rightarrow \infty$) to extremely repelling ($q_2 \rightarrow -\infty$). Figure 1 shows a potential energy surface plot (Figure 1(a)) of \mathcal{V} together with corresponding intersections of it along the q_1 coordinate (Figure 1(b,c)) for various fixed values of the coordinate q_2 .

Focusing on the surface plot of \mathcal{V} one observes that there are three different regions separated by potential barriers. Region I occurs for positive values of q_2 meaning that the SEP has a positive exponent and the motion is confined along the q_1 coordinate. This leads to a channel of the potential clearly visible in Figure 1(a) which extends from $q_2 = 0$ to $q_2 = +\infty$. Consequently the motion inside this confining channel (CC) combines a bounded confined motion of q_1 with an unbounded scattering motion along q_2 , both of them being superexponentially coupled. The latter leads to the fact that the CC is extremely inhomogeneous as can be seen in Figure 1(b) focusing on the intersection curves for positive values of q_2 . For large positive values of q_2 the CC possesses a hard wall box-like confinement which it reaches asymptotically for $q_2 \rightarrow +\infty$ and for which case the q_2 motion is a free ballistic motion decoupled from the q_1 oscillatory box motion. Decreasing the value of q_2 leads to a decrease of the anharmonicity covering continuously all values of the exponent passing on to a harmonic confinement $q_2 = 2$, eventually to a linear one $q_2 = 1$. At $q_2 = 1$ the second derivative $\frac{\partial^2 \mathcal{V}}{\partial q_2^2}$ turns from overall positive to negative with further decreasing values of q_2 . Consequently for $q_2 < 1$ the CC develops a kink at $q_1 = 0$ and flattens out towards a constant potential which it reaches for $q_2 = 0$. Still, the CC maintains an increasingly narrow part around $q_1 = 0$ of significant depth whose width goes to zero for $q_2 \rightarrow 0$.

For $q_2 < 0$ \mathcal{V} exhibits two other distinct regions II and III (see Fig. 1 (a)). They are separated by a potential barrier with a (singular) maximum at $q_1 = 0$. This barrier is naturally of purely repulsive character and widens with a decreasing value of q_2 , while

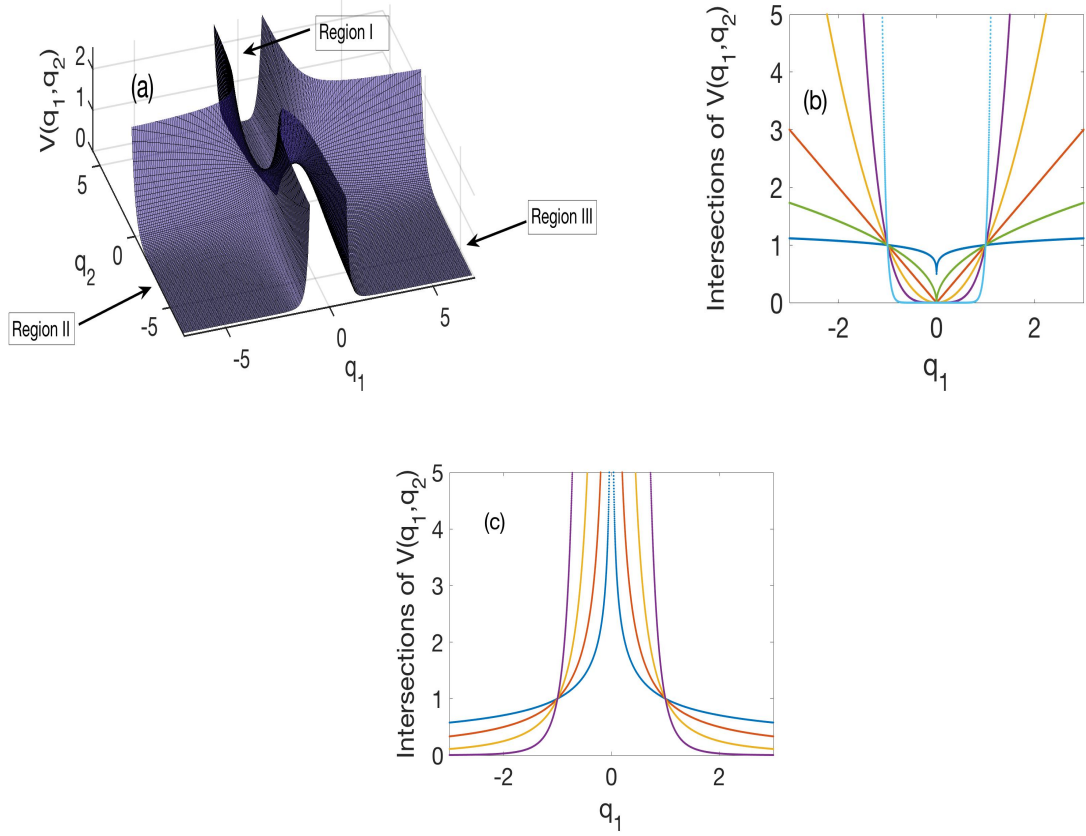


Figure 1. (a) The potential energy surface $\mathcal{V}(q_1, q_2)$. (b) Intersections of the potential energy surface $\mathcal{V}(q_1, q_2)$ along the q_1 coordinate for fixed values of q_2 . Curves from bottom to top in the interval of $-1 < q_1 < 1$ correspond to the values $q_2 = 16, 4, 2, 1, 0.5, 0.1$. (c) same as in (b) but for the values $q_2 = -0.5, -1, -2, -5$.

becoming an infinite repulsive square barrier on the interval $q_1 \in [-1, +1]$ along the degree of freedom q_1 for $q_2 \rightarrow -\infty$ (see Figure 1(c)). In both regions II and III the SEP flattens out with increasing values of $|q_1|$ and a given negative value of q_2 . This implies that the motion in regions II and III becomes asymptotically free. The difference between the two regions is the fact that region II implies that both particles move in a correlated manner to the same direction ($q_1, q_2 < 0$) whereas in region III they move to opposite directions. Region I with the CC motion and regions II and III with an unconfined asymptotically free

motion are separated by two saddle points of the SEP. Taking the partial derivatives of \mathcal{V} and demanding them to be zero yields $q_1 = \pm 1$ and $q_2 = 0$ for the positions of the extrema. The determinant of the corresponding second derivatives is negative thereby providing us with the saddle point character of these extrema. The energies of the saddle points are $E = 1$ and for energies below this energy the motion in the regions I,II,III is disconnected, i.e. an incoming trajectory in the CC would be exclusively reflected (see section III for the investigation of the corresponding dynamics) and not transmitted to the regions II and III with their asymptotically free behaviour. For energies above the saddle point energies transmission is possible and the regions I and II,III are dynamically connected.

In essence, while the appearance of the SEP is strikingly simple it shows an unexpectedly rich geometrical structure with a transition from confined channel motion via saddle points to two distinct regions of asymptotically free motion within which the particles carry different correlations. The intricate highly nonlinear coupling of the degrees of freedom occurring in the SEP is also manifest when formulating it in center of mass and relative coordinates, which are given by $Q = \frac{q_1+q_2}{2}$ and $q = q_1 - q_2$ respectively. The SEP then reads $\mathcal{V} = |Q + \frac{q}{2}|^{Q-\frac{q}{2}}$ which demonstrates the intricate coupling and nonseparability of the center of mass and internal motion of the SEP. Therefore, a treatment in these coordinates does not offer any advantage.

Some notes are adequate at this place. The SEP is neither short-ranged nor long-ranged according to the traditional classification of interaction potentials. It intricately couples the degrees of freedom in a superexponential way thereby enabling the above-discussed variety of behaviour within a simple two-body systems. It combines confining channel and free boundary conditions within a single interaction term. These aspects render the SEP a very promising candidate for a complex geometrical network of corresponding many-body systems as we shall discuss later on in some more detail. The route to complexity is here obviously very much different from some known routes mentioned previously. As a final note we mention that the recently introduced and explored superexponential self-interacting oscillator [13] is a specialization of the present two-body and SEP based problem. Degenerating the two degrees of freedom q_1, q_2 in the sense of the choice $q_1 = q_2 = q$ leads to the one-dimensional interaction potential $\mathcal{V}(q, q) = |q|^q$ whose peculiar properties have been

explored in ref.[13]. We remark that this potential corresponds to the intersection of our SEP potential $\mathcal{V}(q_1, q_2)$ along its diagonal which does not pass through its saddle points.

III. TWO-BODY DYNAMICS FOR SUPEREXPONENTIAL INTERACTIONS

This section is dedicated to the investigation of the dynamics in the SEP. In subsection III A we will first analyze the features of individual trajectories. Our focus is on incoming scattering trajectories in region I i.e. from the asymptotics of the confined channel and for energies below the saddle point energies. In subsection III B the corresponding trajectory ensemble properties are investigated and interpreted. Finally, for energies above the saddle point energies we explore the scattering dynamics of both individual trajectories and in particular of ensembles in the subsection III C: this dynamics connects the channel region I to the asymptotically free motion in the regions II and III.

A. Dynamics in the Confined Channel: Individual Trajectories

The dynamics is described by the Hamiltonian equations of motion belonging to the Hamiltonian (1). To regularize these equations of motion which possess a singularity for $q_2 < 0$ at $q_1 = 0$, we introduce a regularization parameter $\epsilon > 0$ for the SEP which now reads $\mathcal{V}(q_1, q_2; \epsilon) = (\sqrt{q_1^2 + \epsilon})^{q_2}$ and facilitates the numerical integration. This yields the following equations of motion

$$\dot{p}_1 = -\frac{q_1 q_2}{(q_1^2 + \epsilon)} \left(\sqrt{q_1^2 + \epsilon} \right)^{q_2} \quad (2)$$

$$\dot{p}_2 = -\left(\sqrt{q_1^2 + \epsilon} \right)^{q_2} \ln \left(\sqrt{q_1^2 + \epsilon} \right) \quad (3)$$

Typical values for the regularization parameter are $\epsilon = 10^{-8}$. Our numerical results both on the individual trajectory level as well as the ensemble behaviour are independent on this regularization parameter.

We focus in this subsection on incoming ($p_2 < 0$) trajectories in the CC of region I for energies below the saddle point energies. These trajectories are all back reflected within

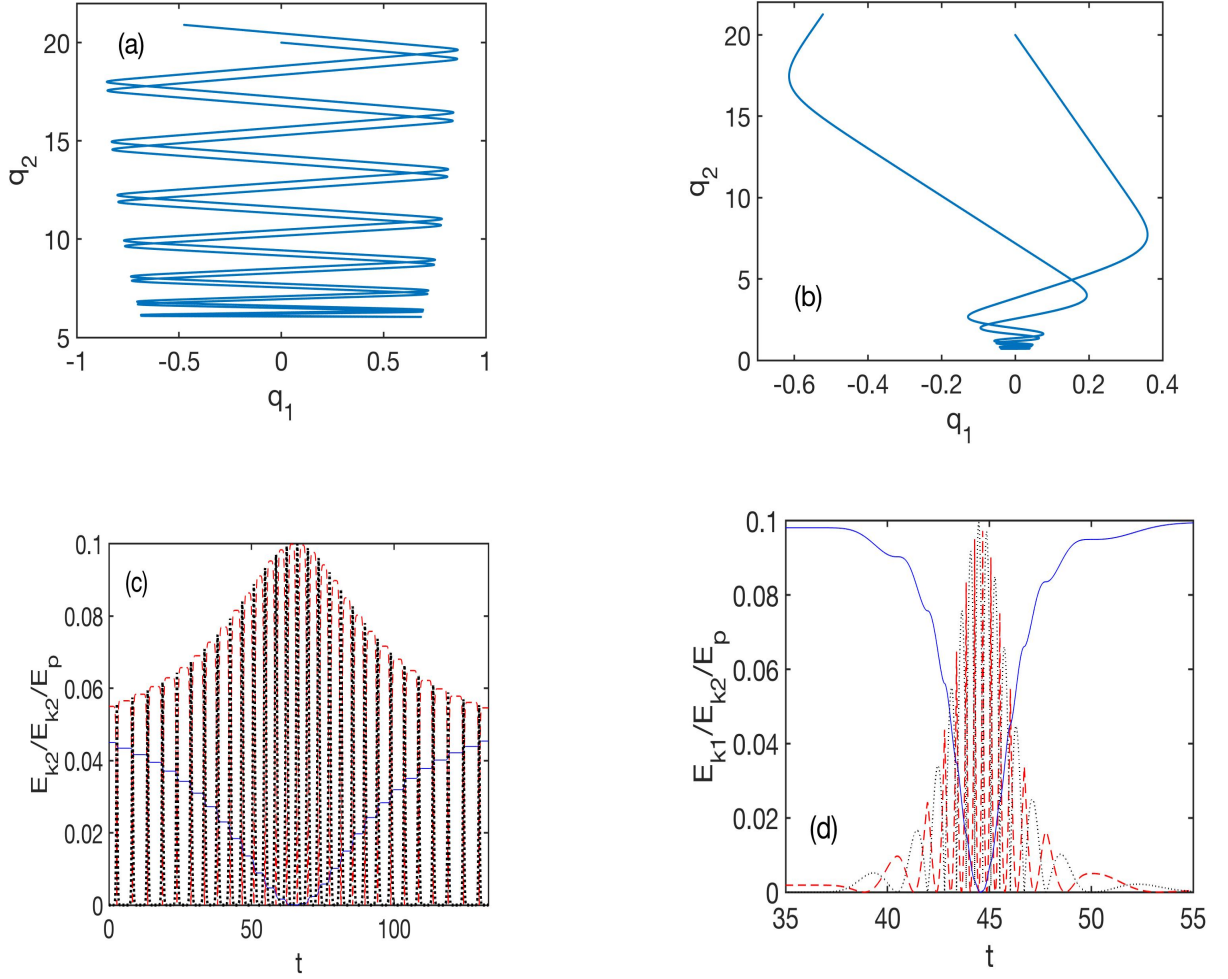


Figure 2. (a) Single trajectory in (q_1, q_2) plane for the initial conditions (incoming channel region I) $q_1 = 0, q_2 = 20, p_2 = -0.3$ for the energy $E = 0.1$. The corresponding time evolution of the kinetic energy $E_{k1} = \frac{p_1^2}{2}$ (red dashed line) and of $E_{k2} = \frac{p_2^2}{2}$ (blue solid line) as well as the potential energy $E_p = |q_1|^{q_2}$ (black dotted line) is shown in subfigure (c). Subfigure (b) shows a corresponding trajectory for the same initial conditions except $p_2 = -0.447$ which is strongly (q_2) forward directed. Subfigure (d) shows the corresponding kinetic and potential energies as in subfigure (c).

the CC and escape asymptotically to $q_2 \rightarrow -\infty$. As indicated above (see section II), the trajectories are initialized for large values of q_2 such that they propagate during the initial phase of their dynamics in an approximately box-like strongly anharmonic channel. In the course of the scattering dynamics the transverse channel confinement continuously changes its exponent ultimately covering all anharmonicities, the close to harmonic case and the linear case while finally developing the above-discussed (see section II) case of $q_2 < 1$ with a flattening and narrowing well around $q_1 = 0$. It depends on the initial conditions, more specifically on the ratio of the longitudinal (p_2) to transverse (p_1) momenta, and on the total energy E what the range of exponents is that is experienced by a specific trajectory. We will focus here on two major examples of individual trajectories, which are the cases of (i) momenta p_1 and p_2 which are comparable in magnitude and (ii) a forward direction scattering process for which $|p_2| \gg |p_1|$. Figures 2(a,b,c,d) show the corresponding motions in the (q_1, q_2) plane together with the time evolution of the kinetic energies $E_{k1} = \frac{p_1^2}{2}$, $E_{k2} = \frac{p_2^2}{2}$ and the potential energy $E_p = |q_1|^{q_2}$.

Figure 2(a) shows a typical trajectory in the (q_1, q_2) plane originating from $q_2 = 20$ with a momentum $p_2 < 0$ according to the above case (i) for a comparatively low energy $E = 0.1$. Starting at the outer parts of the confining channel where the transversal anharmonicity is extremely pronounced and a box-like confinement is present it travels inward (towards $q_2 = 0$) while performing transversal oscillations whose amplitudes decrease with decreasing value of q_2 . At $q_2 \approx 6$ it is backreflected in the channel and travels outward. Figure 2(c) shows the time evolution of the corresponding kinetic E_{k1}, E_{k2} and potential E_p energies. Overall the kinetic energy E_{k1} increases and E_{k2} decreases for the incoming channel trajectory and they exhibit a maximum/minimum at the closest 'collision' point when the trajectory is reflected back. Subsequently the reverse process happens. On top of this envelope behaviour $E_{k1}(t)$ and $E_{k2}(t)$ show a sequence of plateaus with rapid changes in between them. The widths of these plateaus decreases with decreasing value of q_2 and their shape turns into a smooth peak structure. The potential energy $E_p(t)$ mediates the energy transfer between the kinetic energies E_{k1} and E_{k2} and shows pronounced sharp peaks for the times when the transition between the plateaus happens. The plateau structure stems from the traversing of the trajectory of the bottom inner part of the channel during a transversal q_1 oscillation. In this

channel part the potential energy contribution is very small and subsequently each of the kinetic energies E_{k1}, E_{k2} is approximately conserved.

Figure 2(b) shows a trajectory again in the (q_1, q_2) plane emanating in the outer parts of the confined channel but now for the case (ii) of a dominant momentum p_2 . This corresponds to a very much forward (towards the scattering center around $(q_1 = q_2 = 0)$) directed scattering process. As a consequence the trajectory can now enter much deeper into the confining channel in the sense that it experiences the narrowing of the channel for much smaller values of the exponents q_2 . Indeed, Figure 2(b) shows the squeezing of the dynamics impressively i.e. the systematic suppression of the amplitude of the transversal oscillations with decreasing value of q_2 which is the longitudinal channel coordinate. After only a single transversal oscillation the squeezing takes over. The minimal value of q_2 corresponding to the turning point of the motion is now approximately one. As a consequence it can be observed in Figure 2(d) that the plateau structure of the kinetic energies E_{k1}, E_{k2} in case (i) (Figure 2(c)) is no more present in this case but a localized sequence of peaks with strongly varying maximal values in the course of the time evolution. Concerning the flow of energy between the kinetic and potential energies similar statements like the above-ones hold. It is important to note that for both above cases the incoming and outgoing kinetic energies E_{k1}, E_{k2} are approximately equal.

Inspecting incoming trajectories from the (asymptotic) box-like channel one realizes that there is a certain class of trajectories which are reflected back onto themselves in configuration space (q_1, q_2) , which we call return trajectories. Such a case is shown in Figure 3(a) with the same initial conditions as in Figure 2 but for the incoming momentum value $p_2 = -0.4$. Incoming and outgoing channel motion in the (q_1, q_2) plane equal to a very good approximation. Let us analyze this situation in some detail. The turning or closest collision point of a channel trajectory corresponds to the minimum value of q_2 for which $\dot{q}_2(t_0) = 0$. Asking for an exact return trajectory requires to reverse the motion at t_0 which can be shown to yield the condition $\dot{q}_1(t_0) = \dot{q}_2(t_0) = 0$ for the two degrees of freedom q_1 and q_2 . Figure 3(b) demonstrates this for the case of the trajectory shown in Figure 3(a) in the (q_1, q_2) plane. To a very good approximation for this case both velocities $\dot{q}_1 = \dot{q}_2$ becomes zero at the same time $t_0 \approx 52$. The occurrence of such (approximate) return trajectories is supported by the

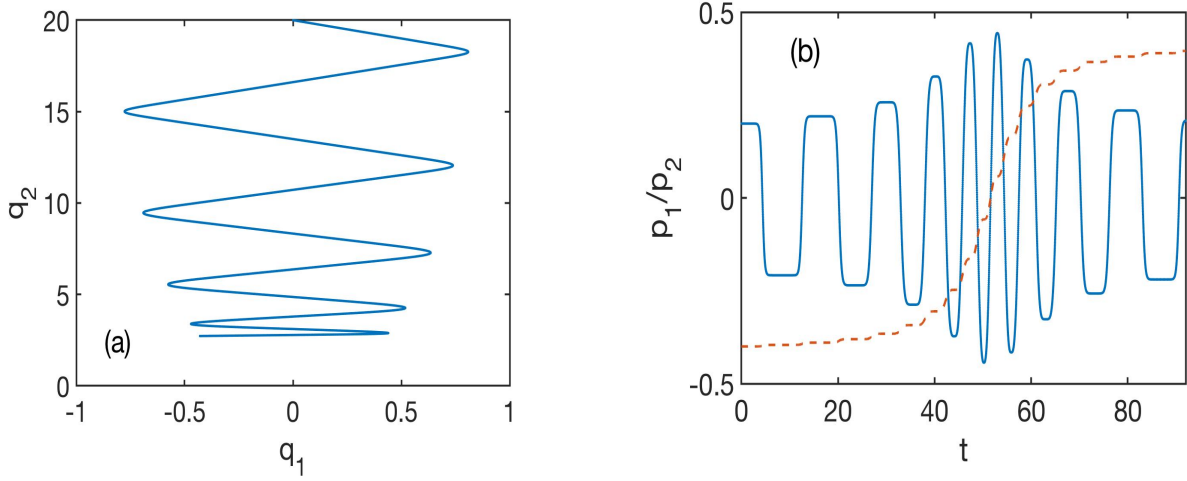


Figure 3. (a) Single return trajectory in (q_1, q_2) plane for the initial conditions (incoming channel region I) $q_1 = 0, q_2 = 20, p_2 = -0.4$ for the energy $E = 0.1$. (b) The corresponding time evolution of the momenta p_1 (blue solid line) and p_2 (red dashed line).

strong oscillatory character of the transversal channel motion $q_1(t)$ rendering it possible to meet the above condition at the turning point of the q_2 -motion. Since the point of return reflection implies the vanishing of both kinetic energies $E_{k1}(t_0), E_{k2}(t_0)$ the total energy is equal to the potential energy $E = E_p(t_0)$. The latter means that the location of this return reflection takes place at the outer parts of the channel where the potential energy becomes significant (see also Figure 3(a)). A channel trajectory that is strongly squeezed (see Figure 2(b)) which enters deep into the region of the narrowed channel is much more sensitive to the detailed initial conditions and consequently the achievement of a return trajectory becomes a fine tuning process.

Let us now focus on large energies of the scattering processes in the channel region I. Figure 4(a) shows a strongly squeezed trajectory for $E = 1$ which is forward focused ($p_2 = -1.414213$). The strong asymmetry for the incoming and outgoing motion, in particular also close to the turning point (see inset of Figure 4(a)), is clearly visible. Figure 4(b) shows the time evolution of a trajectory with $p_2 = -1.122$ for otherwise identical initial conditions and total energy. Here a strong asymmetry with respect to the asymptotic incoming and

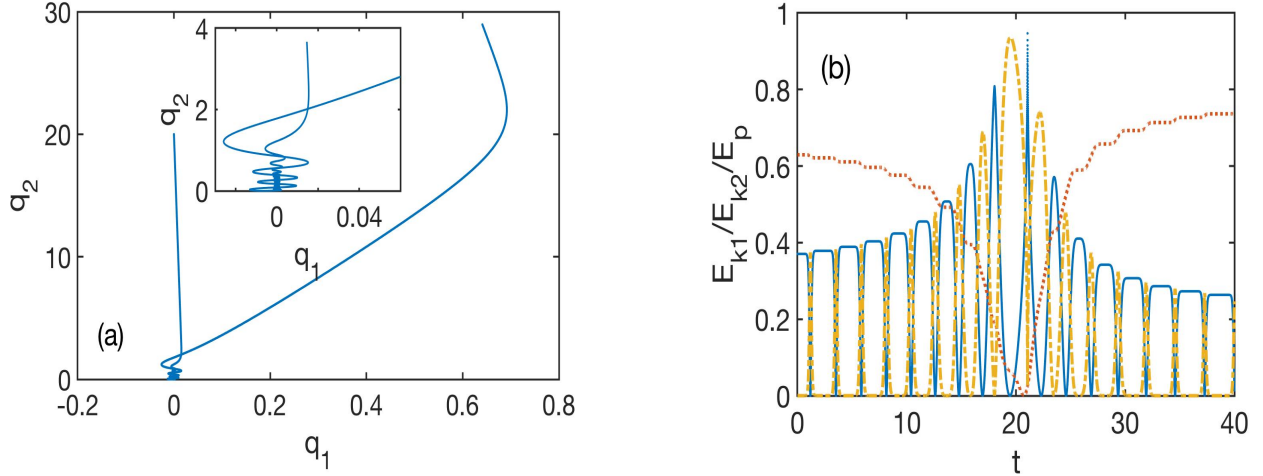


Figure 4. (a) A squeezing trajectory in the (q_1, q_2) plane for the initial conditions (incoming channel region I) $q_1 = 0, q_2 = 20, p_2 = -1.414213$ for the energy $E = 1$. Inset: Magnification around the turning point. (b) Time evolution of the kinetic energies E_{k1} (blue solid line), E_{k2} (red dotted line) and the potential energy E_p (orange dashed dotted line) for $p_2 = -1.122$.

outgoing kinetic energies can be observed which indicates the inelasticity of the underlying process.

B. Dynamics in the Confined Channel: Ensemble Properties

Lets explore the properties of ensembles of trajectories in order to gain a representative view on the dynamics. In this subsection we focus on the confining channel of region I. We fix q_1, q_2 initially and random uniformly distribute the kinetic energy E_{k2} (both the initially incoming and finally outgoing trajectory values for q_2 are fixed to 20 which is sufficiently close to the asymptotic channel region where the transverse q_1 profile of the SEP is box-like). E_{k1} is then adapted to the energy shell and also uniform randomly distributed. The random distribution of the corresponding momenta p_1, p_2 follows then a (piecewise) linear envelope. We proceed by first analyzing the case of low energies followed by higher energies in the confined channel.

We will proceed as follows in this subsection. First we will discuss the main features

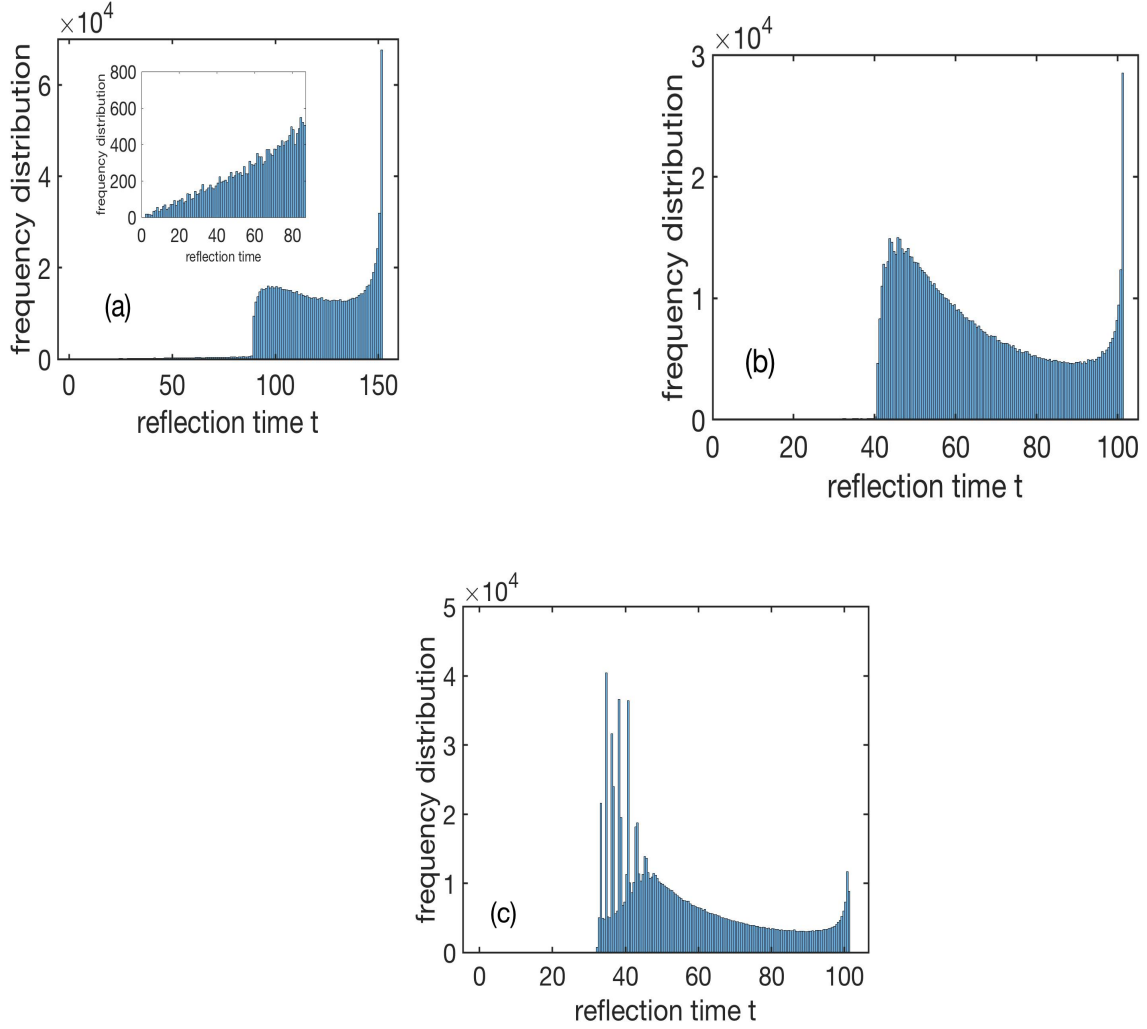


Figure 5. (a) Reflection time distribution for scattering in the confining channel (region I) for $E = 0.1$. The ensemble of 10^6 trajectories obeys the initial conditions $q_1 = 0, q_2 = 20$ and the kinetic energies are chosen uniform randomly. (b,c) Same as (a) but for $E = 0.5$ and $E = 0.8$ respectively.

of the reflection time distribution for the scattering in the confined channel. In a second step it will be analyzed by employing so-called correlation diagrams. Subsequently we will explore the in-out scattering functions followed by an analysis of the final kinetic energy distributions.

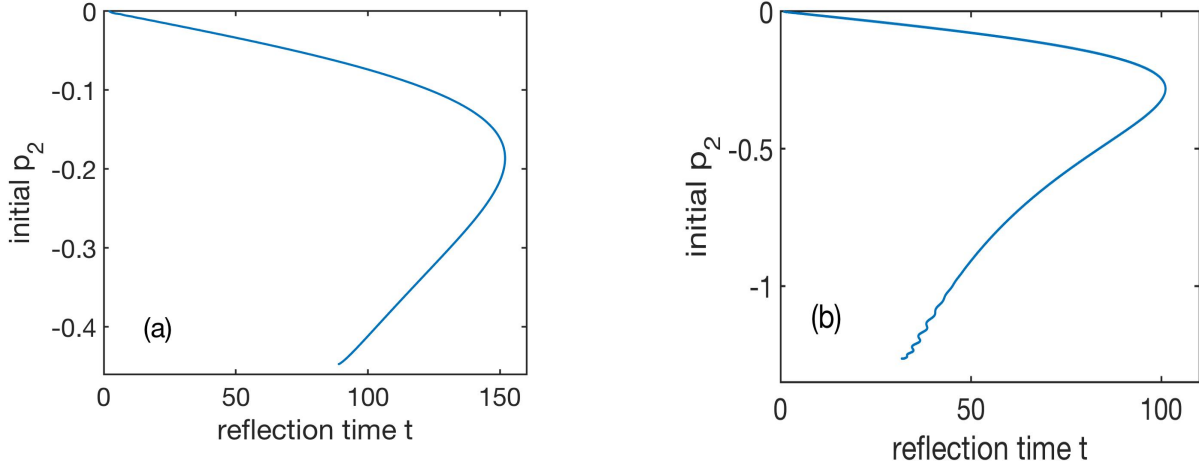


Figure 6. (a) Correlation diagram of the initial momentum p_2 versus the reflection time for $E = 0.1$. (b) same as in (a) but for $E = 0.8$.

1. Features of the reflection time distribution

Figure 5 shows the reflection time distribution (RTD) for an ensemble of 10^6 trajectories. Inspecting the case $E = 0.1$ in Figure 5(a) our first observation is that the resulting frequency distribution exhibits two plateaus and a dominant peak. For small reflection times $t < 90$ the RTD is strongly suppressed (see inset of Figure 5(a)) and the distribution increases linearly with an increasing reflection time. One reason for this behaviour is the fact that the initial ($t = 0$) momentum distribution of p_2 goes linearly to zero at $p_2 = 0$ and therefore small forward momenta tentatively resulting in small reflection times are suppressed. At $t \approx 87$ (see Figure 5(a)) a sudden rise occurs for the RTD to a plateau of reflection times larger by more than an order of magnitude as compared to small reflection times. On this plateau the RTD shows a smooth oscillation with further increasing reflection time that is stretched significantly towards larger reflection times. Then, for the maximum reflection time $t \approx 155$ a dominant narrow peak is encountered.

2. Analysis via the correlation diagram

What is the origin of the above features and in particular of the plateau structure of the RTD ? To address this question, the correlation diagram of the reflection time depending on the initial momentum $p_2(t=0)$ is very instructive. Figure 6(a) shows this dependence for the energy $E = 0.1$. We observe that the 'mapping' of the initial momentum onto the reflection time is represented by a well-defined curve. For small reflection times $t \lesssim 87$ this curve is single-valued which is identical to the regime of the first plateau of reflection times of the RTD for low values. From $t \approx 88$ on a double valuedness occurs i.e. there are two initial momentum branches that contribute to a certain interval of reflection times. At $t \approx 88$ the second (lower) branch starts at the most negative possible value for the initial momentum $p_2(t=0)$ and moves to less negative values with further increasing reflection time t . The latter momenta $p_2 \gtrsim -0.45$ possess a very high probability in the initial uniform random ensemble and represent therefore a major reason for the above-mentioned step-like increase of the RTD. The point of the appearance of the second branch in the (p_2, t) correlation diagram is the point of the appearance of trajectories that, starting at $t = 0$ from $(q_1 = 0, q_2 = 20)$, travel all the way to the origin of the SEP (note that $\mathcal{V}(q_1 = 0, q_2) = 0, \forall q_2 > 0$). Since $E = E_{k2}$ holds in this case, i.e. all energy is kinetic energy of the degree of freedom q_2 . The time for the occurrence of this trajectory is straightforwardly determined to be $t \approx 89$ which agrees with the above-observed value. The second lower branch of strongly negative values of $p_2(t=0)$ represents a second dominant contribution to the reflection times beyond $t \approx 90$, whereas the upper branch exists already for $t < 90$ and adds low probability to the RTD.

The stretched oscillatory behaviour of the second plateau of the RTD in Figure 6(a) can be understood by the different slopes of the two branches contributing to the statistics of the reflection time. The lower branch possesses a steeper slope compared to the upper branch and its contribution to the RTD thereby decreases more rapidly with increasing reflection time as compared to the corresponding impact of the weaker slope of the upper branch. This leads on the second plateau to an overall decrease of the RTD. The peak structure for even larger reflection times becomes here also understandable since the momentum branch

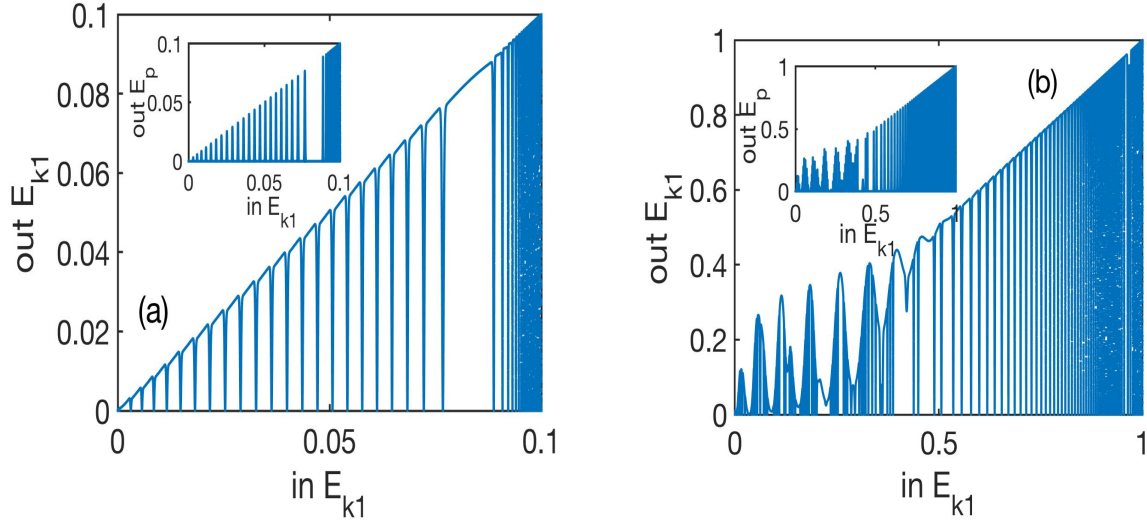


Figure 7. (a) In-out scattering function for the kinetic energy E_{k1} for $E = 0.1$. Inset: Scattering function of incoming E_{k1} and outgoing E_p . Initial conditions and ensemble properties as indicated in Figure 5. (b) and its inset: Same as in (a) but for $E = 1$.

becomes tangentially vertical and therefore a broad range of momenta contribute to the maximal reflection time. We note that the neighborhood of the onset of the lower branch in the correlation diagram (p_2, t) corresponds to strongly squeezed trajectories as discussed in subsection III A.

3. In-out scattering functions

Sticking with the energy $E = 0.1$ let us analyze some relevant in-out scattering functions related to the different kinetic and potential energies. Figure 7(a) shows the scattering function, i.e. in-out mapping, of the kinetic energy E_{k1} . Since at $t = 0$ we have $E_p = 0$ and $E = E_{k1} + E_{k2}$ the initial E_{k1} directly translates to E_{k2} . We observe that the outgoing E_{k1} is proportional to the initial incoming E_{k1} interrupted by narrow dips or antipeaks. These antipeaks correspond to the situation where the outgoing potential energy becomes maximal, see inset of Figure 7(a). This happens, due to the flatness of the bottom of the outgoing transversal potential well ($q_2 = 20$) and the corresponding steep walls, only if the

phase of the transversal q_1 oscillation of the outgoing trajectory is such that the particle coordinate q_1 encounters those steep walls and converts its kinetic to potential energy. This process happens repeatedly when, in the above sense, phase matching is encountered. Of course, the concrete value of the outgoing phase is determined also by the detailed scattering dynamics at small(er) values of q_2 .

For large kinetic energies E_{k1} first an energetic gap with no (anti-)peaks occurs and subsequently an accumulating series of antipeaks for E_{k1} and of peaks for E_p is encountered (see Figure 7(a)). This accumulation originates from the fact that the slow q_2 -motion for large kinetic energies E_{k1} and the resulting high frequency q_1 oscillations lead to an increasingly rapid change of the phase of the outgoing trajectory with varying E_{k2} . These rapid phase changes lead also to a series of peaks with large potential energies E_p due to the repeated 'collisions' with the transverse potential walls for the outgoing large q_2 -value. The upper branch in the correlation diagram in Figure 6(a) shows for small reflection times an approximately linear behaviour of p_2 as a function of the reflection time. The corresponding kinetic energies E_{k1}, E_{k2} scale then quadratically with the reflection time for sufficiently small initial momenta p_2 . The accumulation of peaks at $E_{k1} = 0.1$ (see Figure 7(a)) is connected to this quadratic scaling: varying $E_{k2} \propto t^2$ linearly leads to a corresponding nonlinear phase change and accumulation of peaks. A final note is in order concerning the conversion of the kinetic energy to potential energy in the course of the transversal channel dynamics. A brief calculation shows that the ratio of the forces acting on the two degrees of freedom (q_1, q_2) reads as follows

$$\frac{\dot{p}_1}{\dot{p}_2} = \frac{q_2}{q_1 \ln |q_1|} \quad (4)$$

which indicates that the force acting on q_1 dominates the force acting on q_2 at our incoming/outgoing boundary since $q_2 \gg |q_1|$. Therefore, the changes of the motion of q_1 are decisive for the conversion of the corresponding kinetic energy to potential energy.

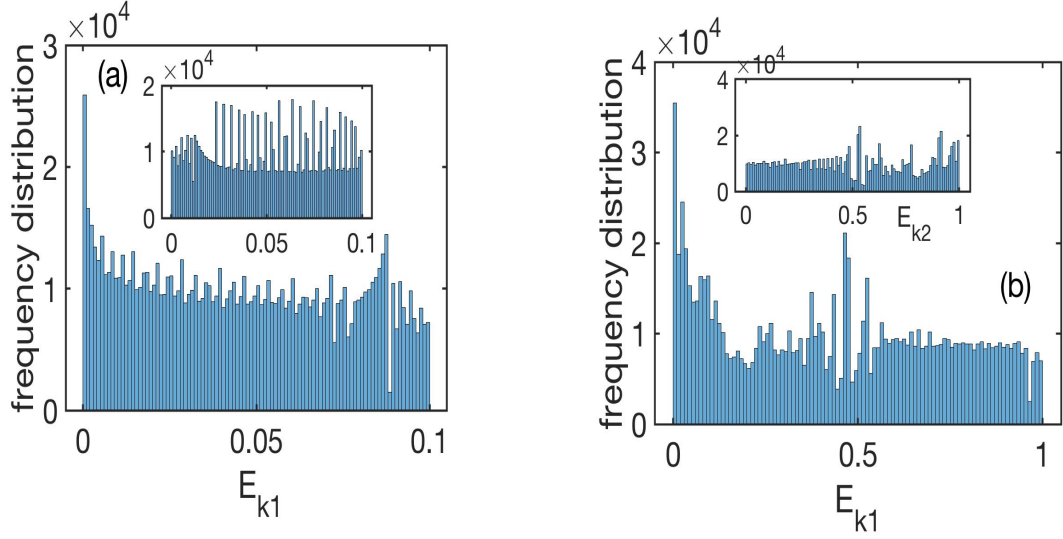


Figure 8. (a) Outgoing kinetic energy distribution of E_{k1} for an ensemble of 10^6 trajectories with the initial conditions $q_1 = 0, q_2 = 20$ for $E = 0.1$ and uniform randomly chosen initial kinetic energies E_{k1}, E_{k2} . Inset: Corresponding outgoing kinetic energy distribution for E_{k2} . (b) Same as in (a) but for $E = 1$.

4. Kinetic energy distributions

We explore now the outgoing kinetic energy distributions (KED) E_{k1}, E_{k2} of the scattering of the ensemble of trajectories in the CC in region I. Figure 8(a) shows these KED in the main figure and inset for a total energy of $E = 0.1$. Opposite to the uniform initial KED the scattered distributions exhibit several pronounced structural features. In particular we observe an oscillatory progression of fluctuations with increasing kinetic energy E_{k1} and correspondingly E_{k2} (see inset). Narrow and broad peaks are located at the maximal and minimal values of the kinetic energies, to a lesser extent at intermediate values. Besides high frequency oscillatory structures also asymmetric peaks of one-sided smooth character appear, extending over a broader interval of energies. These oscillations observed in the KED correspond to the oscillations observed in the kinetic energy scattering functions discussed above (see Figure 7(a)). An enhanced probability of the KED occurs if the outgoing kinetic energy integrates over the rapidly varying antipeaks.

Let us now focus on the case of higher energies thereby addressing the most important changes as compared to the above discussion for $E = 0.1$. For the RTD in Figure 5(b) ($E = 0.5$) we observe that the stretched oscillation occurring for $E = 0.1$ at the location of the second plateau develops into a deep valley while at the same time the corresponding correlation diagram $(p_2(t = 0), t)$ deforms (not shown here for brevity). Moving on to the case $E = 0.8$ the RTD (see Figure 5(c)) shows now at the point of the appearance of the lower branch of the corresponding correlation diagram (see Figure 6(b)) a series of major peaks which stem from the oscillatory behaviour at the beginning of this branch in the correlation diagram. The latter can be understood by noticing that the contributions to the RTD stem either from straight monotonic parts of the initial momentum p_2 (low values of reflection time probability) or from parts around the turning point (high values of reflection time probability). The oscillations in the correlation diagram therefore directly translate to the peaks of the RTD. In Figure 7(b) these modulations are reflected in the in-out mapping of the kinetic energy distribution for E_{k1} (for $E = 1$). In the corresponding inset of Figure 7(b) the modulations leave their fingerprints in the peak structure of the in-out mapping of E_{k1} to E_p . The outgoing KED for $E = 1$ develops equally a highly fluctuating behaviour.

C. Dynamics Above the Saddle Points

We now investigate the dynamics for energies above the two saddle points, for which case both reflection and transmission is possible. Our trajectories are initialized again in the CC in region I of the SEP for comparatively large values of q_2 where the transverse profile of the channel is already box-like. We will first inspect a few prototype trajectories and then focus on the ensemble properties. The primary quantity of interest is the scattering distribution with respect to the angle $\Phi = \arccos\left(\frac{q_1}{q_1^2 + q_2^2}\right)$ and the fraction of reflected versus left (region II) and right (region III) transmitted trajectories with varying energy. Obviously, Θ characterizes the direction of scattering among the two degrees of freedom q_1, q_2 .

Figure 9 illustrates three prototypical trajectories in the (q_1, q_2) plane for an energy $E = 1.2$ above the saddle points. While one of them is backreflected into the CC, the other two are transmitted, one of them to region II and the other one to region III. As indicated

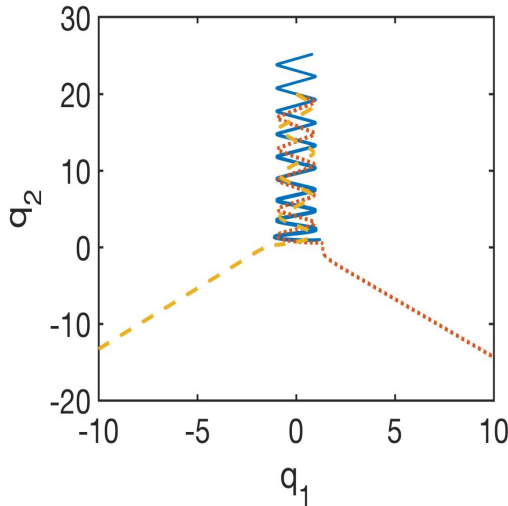


Figure 9. Three example trajectories in the (q_1, q_2) plane for initial conditions $q_1 = 0, q_2 = 20$ and $p_2 = -0.9, -1.1, -1.3$ for an energy $E = 1.2$ above the saddle point energies. The back reflection (region I) as well as the left (region II) and right (region III) transmission processes are demonstrated.

previously (see section II), region II ($q_1 < 0, q_2 < 0$) implies that the two particles move in a correlated manner in the same direction whereas region III ($q_1 > 0, q_2 < 0$) is responsible for processes where both particles move in opposite directions. The dynamics in the vicinity of the saddle points leads to the branching to one of these regions. Back reflection means that the particle with coordinate q_2 leaves with an asymptotically free motion to $-\infty$ whereas the second particle remains in an oscillating state. Transmission yields then freely propagating particles asymptotically. In this sense a deconfinement transition happens that turns the q_1 degree of freedom which is strongly confined in region I and strongly nonlinearly coupled to the q_2 degree of freedom after passing via the saddle point to a free degree of freedom. This means a dynamical unfolding of the confined degree of freedom q_1 while passing from the channel region via the saddle points to the unconfined and asymptotically free region. The two regions II and III are separated by a (singular) barrier centered around $q_1 = 0$ which becomes an infinite square barrier asymptotically for $q_2 \rightarrow -\infty$.

Figure 10(a) shows the scattering angular distribution (SAD) for an energy $E = 1.5$ slightly above the saddle point energies. Three isolated peaks can be observed. The one lo-

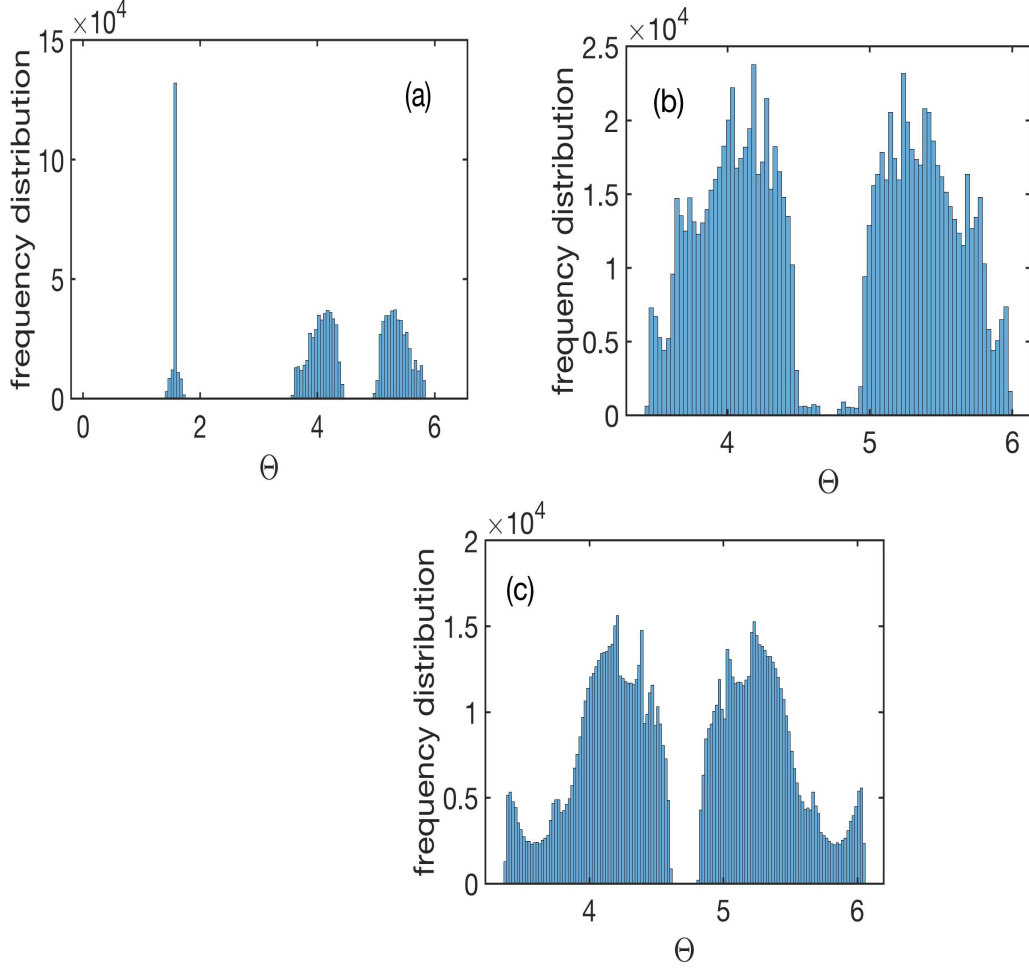


Figure 10. Angular distribution functions of the scattering process for an ensemble of 10^6 trajectories injected from the CC in region I for the initial conditions $q_1 = 0, q_2 = 20$ for the energies $E = 1.5, 2.5, 5.5$ in (a),(b),(c) correspondingly, which are above the saddle point energies. Θ is provided in radian units.

cated at $\frac{\pi}{2}$ is the dominant and narrowest peak. It corresponds to trajectories backscattered into the CC. The other two smoother and broader peaks correspond to the transmission scattering into the asymptotic regions II and III respectively. They are centered around 1.3π and 1.7π respectively. Generally with increasing energy the height of the back scattering peak decreases, while for the forward scattered distributions the corresponding widths increase and the shape becomes increasingly asymmetric while the maximal values increase too.

Focusing on the SAD in Figure 10(b) for $E = 2.5$ the backscattering peak has disappeared completely and two very broad distributions in the corresponding sectors of region II and III have emerged. They almost overlap (note that there is an impenetrable barrier between them) and possess a characteristic asymmetric overall shape imprinted by the presence and shape of the barrier: a steep slope occurs around $\Theta = \frac{3\pi}{2}$ and a smoother decay for the outer part of the distributions, though modulated by additional peaks. Finally, for even higher energies (see Figure 10(c) for $E = 5.5$) the distributions develop a dynamically induced modulation.

IV. CONCLUSIONS AND OUTLOOK

We have performed in this work a first step on the route to form complex structures from fundamental building blocks with superexponential interactions by exploring a system of two degrees of freedom. The underlying superexponential potential is of very simple appearance but shows an amazingly rich behaviour and properties. Opposite to common two-body problems with e.g. Coulomb or dipolar interaction potentials depending on the relative coordinates of the two particles, the superexponential potential puts the nonlinearity to the extreme: the base of its exponential dependence and the exponent depend on the dynamical degrees of freedom. Resultingly the SEP is inherently inseparable, highly asymmetric and nonlinear and does not obey the standard asymptotic boundary conditions. Specifically we have shown that the SEP exhibits three different regions with a qualitatively different geometry and coupling of the degrees of freedom. In the so-called region I we encounter a confined channel geometry along which the transversal confinement continuously changes its anharmonicity from box-like in the asymptotics to an inverse cusp structure close to the origin. This channel is connected via two saddle points to the regions II and III which are separated by a repulsive barrier. In the latter regions the dynamics is asymptotically free and corresponds to a correlated motion in the same or opposite directions of the two degrees of freedom respectively. The scattering dynamics initialized in the confining channel therefore leads for energies above the saddle points to a deconfinement transition and finally to asymptotic freedom. In this sense the originally confined degree of freedom is dynamically

unfolded within the highly nonlinear scattering process.

More specifically we have explored the scattering dynamics in the confining channel below and above the saddle point energies for several relevant observables. The transition from a box-like to an extremely squeezed channel towards the scattering center leads to a characteristic energy exchange pattern of series of plateaus converging to a sequence of highly localized peaks. The reflection time statistics of the corresponding ensembles show two major plateaus for low energies which can be analyzed and understood by employing corresponding correlation diagrams between the initial momentum and the reflection time. For higher energies additional peak structures occur. The dynamics above the saddle points connects the channel region with the transmission regions and our analysis of the resulting angular distribution functions identifies the characteristics of this scattering with varying energy.

This work represents the basis for many possible extensions to come. Our interaction potential $\mathcal{V}(q_1, q_2) = |q_1|^{q_2}$ is nonreciprocal i.e. it doesn't treat the two degrees of freedom on an equal footing. A natural extension of the SEP would therefore be to symmetrize it yielding $\mathcal{V}_s(q_1, q_2) = |q_1|^{q_2} + |q_2|^{q_1}$. This interaction potential possesses more than one channel and resultingly an even more intricate dynamics as compared to the presently treated nonreciprocal case. Investigating this setup therefore goes beyond the scope of this work. Our two degrees of freedom system represented by a single SEP term, can be extended in multiple ways to several degrees of freedom. Indeed, the coupling between the exponent degrees of freedom and the base degrees of freedom can be chosen in different ways, such that the analogue of artificial 'atoms', 'molecules', 'chains' or 'clusters' of networks of channels and regions of free motion being connected by saddle points could be imagined. Second the dependence on the absolute coordinates seems to be very natural, but not the only possibility: relative coordinate dependencies might introduce a qualitatively different behaviour. The generalization to higher dimensions opens the route to exploit radial and angular coordinate dependencies in order to control possible anisotropies.

Finally the question can be posed what physical systems can potentially be described by our superexponential interaction profile. While we do not have a conclusive answer to this question it is conceivable that the SEP is a result of an effective description of an already

complex system consisting of many cooperative degrees of freedom. On the other hand the dynamical degrees of freedom appearing in the SEP could also describe the motion in some parameter or effective space and not the real coordinate space.

V. ACKNOWLEDGMENTS

This work has been in part performed during a visit to the Institute for Theoretical Atomic, Molecular and Optical Physics (ITAMP) at the Harvard Smithsonian Center for Astrophysics in Cambridge, Boston, whose hospitality is gratefully acknowledged. The author thanks F.K. Diakonos and B. Liebchen for a careful reading of the manuscript and valuable comments.

-
- [1] H. Friedrich, Theoretical Atomic Physics, Springer International Publishing 4th ed. 2017.
 - [2] T. Helgaker, P. Jorgensen and J. Olsen, Molecular Electronic Structure Theory, John Wiley and Sons, 2nd ed. 2020.
 - [3] J. Jellinek, Theory of Atomic and Molecular Clusters, Springer New York 1999.
 - [4] D. Natelson, Nanostructures and Nanotechnology, Cambridge University Press, Cambridge 2015.
 - [5] N.W. Ashcroft and N. Mermin, Solid State Physics, Brooks Cole Publishing Company, Singapore, 2018.
 - [6] E.B. Wilson, J.C. Decius, P.C. Cross, Molecular Vibrations: The Theory of Infrared and Raman Vibrational Spectra, Dover Books on Chemistry, 1980.
 - [7] M. Tabor, Chaos and Integrability in Nonlinear Dynamics, John Wiley and Sons (1989).
 - [8] S.H. Strogatz, Nonlinear Dynamics and Chaos: With Applications to Physics, Biology, Chemistry, and Engineering (Studies in Nonlinearity), Westview Press 2nd Edition (2015).
 - [9] L.E. Reichl, The Transition to Chaos, 2nd edition Springer (2004).
 - [10] S. Flach, C.R. Willis, Phys.Rep. 295, 181 (1998).

- [11] L.S. Cao, D.X. Qi, R.W. Peng, Mu Wang, and P. Schmelcher, Phys.Rev.Lett. 112, 075505 (2014).
- [12] P. Schmelcher, Phys. Rev. E 98, 022222 (2018).
- [13] P. Schmelcher, arXiv:1909.09792, acc.f.publ. J.Phys.A